First-principles investigations of multimetallic transition metal clusters

Peter Entel, Markus E. Gruner, Georg Rollmann, Alfred Hucht, Sanjubala Sahoo, Alexey T. Zayak, Heike Herper, Antje Dannenberg

First-principles investigations of multimetallic transition metal clusters

Journal:	*Philosophical Magazine & Philosophical Magazine Letters*
Manuscript ID:	TPHM-08-May-0181
Journal Selection:	Philosophical Magazine
Date Submitted by the Author:	21-May-2008
Complete List of Authors:	Entel, Peter; Univ. Duisburg-Essen, Duisburg Campus, Department of Physics Gruner, Markus; Univ. Duisburg-Essen, Duisburg Campus,, Department of Physics Rollmann, Georg; Univ. Duisburg-Essen, Duisburg Campus, Department of Physics Hucht, Alfred; Univ. Duisburg-Essen, Duisburg Campus,, Department of Physics; Univ. Duisburg-Essen, Duisburg Campus, Department of Physics Sahoo, Sanjubala; Univ. Duisburg-Essen, Duisburg Campus,, Department of Physics Zayak, Alexey; University of Texas at Austin, Institute for Computational Engineering and Science Herper, Heike; University of Duisburg-Essen, Theoretical Physics Dannenberg, Antje; Univ. Duisburg-Essen, Duisburg Campus,, Department of Physics
Keywords:	ab initio, clusters, transition metals
Keywords (user supplied):	ab initio, clusters, transition metals
Note: The following files were submitted by the author for peer review, but cannot be converted to PDF. You must view these files (e.g. movies) online.	
iccm-entel 0808.tex	

Philosophical Magazine
Vol. 00, No. 00, 00 Month 200x, 1–11

RESEARCH ARTICLE

First-principles investigations of multimetallic transition metal clusters

P. Entel[a]* M.E. Gruner[a], G. Rollmann[a], A. Hucht[a], S. Sahoo[a], A.T. Zayak[b], H.C. Herper[a] and A. Dannenberg[a]

[a]*Physics Department and Center for Nanointegration CENIDE, University of Duisburg-Essen, 47048 Duisburg, Germany*
[b]*Institute for Computational Engineering and Science, 201 East 24th Street ACES, University of Texas at Austin, Austin, Texas 78712, USA*

(*Received 00 Month 200x; final version received 00 Month 200x*)

This brief overview summarizes state-of-the-art of simulations of transition metal nanoclusters based on density functional theory calculations. Besides the monometallic clusters like iron, we focus on alloy nanoclusters like Fe-Pt, Co-Pt and (Ni, Co)-Mn-Ga which are of current interest for recording media and actuators involving the magnetic shape memory effect, respectively. Although catalysis it is not subject of the present paper, trimetallic nanoclusters are of special interest because the third element can be used to achieve higher catalytic and selective properties compared to the corresponding monometallic and bimetallic clusters. For clusters of Fe-Pt and Co-Pt below a critical size, the $L1_2$ structure with its technologically relevant high magnetocrystalline anisotropy is difficult to stabilize. For trimetallic systems like Ni-Mn-Ga, the rather versatile properties of the bulk material can be used to achieve shape changes or magnetocaloric effects (depending on the composition) also in nanoclusters. Important is here that it might be cheaper to manufacture the nanocrystalline materials from the trimetallic nanoclusters than to fabricate corresponding single-crystal bulk systems.

1. Introduction and computational details

The broad range of potential applications of metallic clusters and thin metallic films in nanomagnetism [1], spintronics [2] or multiferroic [3] devices has lead to increasing research activities over the last decade. The exchange bias in small particles, ferromagnetic (FM) particles covered by their antiferromagnetic (AFM) or ferrimagnetic native oxide like Co-CoO [4] or in layered antiferromagnetic-ferromagnetic structures [5] has been proposed or used in different applications, see [4] for references. Progress in spintronics will probably only be achieved - if in addition to charge current - one will understand how to manipulate and control the spin current in the nanodevices important for the spin Hall effect [6]. Another field of applications is alloying of clusters which makes them more complex than monometallic clusters but in particular renders them more interesting for catalysis because of their much higher catalytic activity compared to the corresponding monometallic clusters [7]. Thus, a further technological breakthrough of using nanoparticles on a large scale can be expected from their ability to speed up catalytic reactions.

Therefore, we concentrate in this paper on multimetallic (Fe, Co)-Pt and (Ni, Co)-Mn-Ga nanoclusters. In particular, we are interested in the influence of magnetism on the compositional ordering and phase separation. Different morphologies of the clusters as function of the cluster size will also influence the catalytic behavior of the clusters. But here we are not so much interested in nanoparticle catalysis but on the ability of (Fe, Co)-Pt and (Ni, Co)-Mn-Ga to act in storage media [8], magnetic shape memory [9] and magnetocaloric [10] devices, respectively. As an introduction we will discuss the physical

*Corresponding author. Email: peter.entel@uni-due.de

ISSN: 1478-6435 print/ISSN 1478-6443 online

DOI: 10.1080/1478643YYxxxxxxxx
http://www.informaworld.com

properties of monometallic Fe nanoclusters because they are one of the rare examples which explicitely allows to illustrate the influence of magnetism on the cluster growth.

Most of the results for the bimetallic clusters discussed below have been obtained from large-scale *ab initio* investigations carried out on the IBM Blue Gene/L and Blue Gene/P supercomputer systems of the John von Neumann Institue for Computing at Forschungszentrum Jülich. In the density funtional theory calculations we mainly used the Vienna *ab initio* simulation package (VASP) [11] and the projector augmented wave approach [12] with a sufficiently high plane wave cut-off energy and k-space integration restricted to the Γ-point. The size of the supercell containing the nanoparticle was chosen such that the distance between atoms of the periodic images was exceeding 9 Å. All nanoclusters were allowed to perform structural relaxations. For further computational details we refer to [13–15], where part of the results discussed below have been published.

The electronic structure calculations for the ternary magnetic Heusler clusters were mainly undertaken using density functional theory method in real-space on a fine grid with spacing of 0.1 Å and the high-order finite difference method as implemented in the code PARSEC [16]. For computational details involving Heusler clusters cut from the half-metallic bulk material, see [17], for computational details involving the magnetic shape memory nanoclusters, see [18].

2. Monometallic Fe clusters

Iron and iron-oxide nanoparticles are biocompatible and non-toxic. They show a variety of features which have made them a playground both in experimental [19–23] and in theoretical investigations [24–26]. Among the amazing properties one finds that the magnetic moment depends stongly on the morphology and size of the clusters [19, 24, 25]. On the other hand, the shape controlled synthesis of of iron-oxide nanoparticles offers the possibility for cubic, spherical and other morphologies [20]. So, tayloring of magnetic and structural properties of the particles for storage devices in the nanorange may be possible. Intriguing is also the formation of chain- and knot-like structures (self-assembled Fe nanowires) in the gas phase or on substrates [21–23] where structure formation is essentially dominated by the long-range dipolar interaction between the magnetic nanoparticles. The generic phase diagram of how these structures emerge either as a function of the temperature or the external magnetic field has recently been established [26].

Another recent observation is that magnetism and growth of iron nanoclusters are interrelated. For cluster sizes consisting of more than ca. 147 Fe atoms, the bcc-related cluster structures are energetically more favorable than other isomers [13]. This shows that already small Fe clusters tend towards the bcc geometry corresponding to the ground state structure of FM bulk iron [13]. Other morphologies, especially of icosahedral form, may undergo a partial (shellwise) transformation along the Mackay-path which connects icosahedra and fcc-like cuboctahedral isomers [27]. The latter may transform to the bcc structure following essentially the Bain path [28]. Figure 1 illustrates the Mackay transformation from the perfect icosahedron to the perfect cuboctahedron and the initial fcc structure for the fcc $\rightarrow$ bcc Bain transformation. Within the shellwise Mackay transformation (SMT) each of the completed geometric shells of the cluster transforms to a different degree, the inner shell of the nanoclusters shows cuboctrahedral (fcc) structure while the outer shells remain icosahedral. This can be described by the parameter s defined as squared ratio of the two characteristic lengths in Fig. 1,

$$s = \left(\frac{\overline{AC}}{\overline{\overline{AB}}}\right)^2 = \begin{cases} 1 : \mathrm{I}CO \\ 2 : CUBO \end{cases}$$

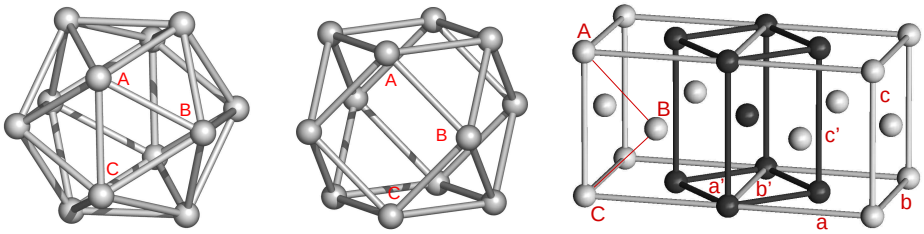

Figure 1. Left and center: Icosahedron and cuboctahedron - during the Mackay transformation, the bond $\overline{AC}$ (left) stretches and the two adjacent triangles turn into the same plane. The capital letters refer to the same atomic sites in each structure. Right: Face-centered cubic lattice with inscribed body-centered tetragonal Bain cell. The Bain transformation is controlled by variation of c with respect to a and b. Figure adapted from [13], copyright (2007) by the American Physical Society.

where ICO and CUBO stand for perfect icosahedron and cuboctahedron, respectively.

Although the SMT morphologies are only metastable states for $N \geq 147$, they represent quite robust local minima in the potential energy landscape. In fact, cuboctahedra and icosahedra turn out to be instable against a transformation if slight distortions along the Mackay path are imposed. This is demonstrated in Fig. 2 for the case of a 147 atom Fe cluster, which consists of three closed geometric shells. Here, the evolution of three differently initialized Fe_{147} isomers during *ab initio* conjugate gradient optimizations procedures are compared. The degree of transformation is determined individually for each shell by computing s, i.e., the squared ratio between the distances of the corner atoms belonging to the square facets of the cuboctahedron or the corresponding two adjacent triangular facets of the icosahedron, respectively, as depicted in Fig. 1. Already after a few steps (in the order of 20) all three structures reach essentially the same SMT structure, characterized by the different transformation degrees corresponding to each shell, ranging from mostly icosahedral for the innermost shell to predominantly cuboctahedral for the outermost shell.

A common neighbor analysis [31] reveals that this results in bcc-like environments

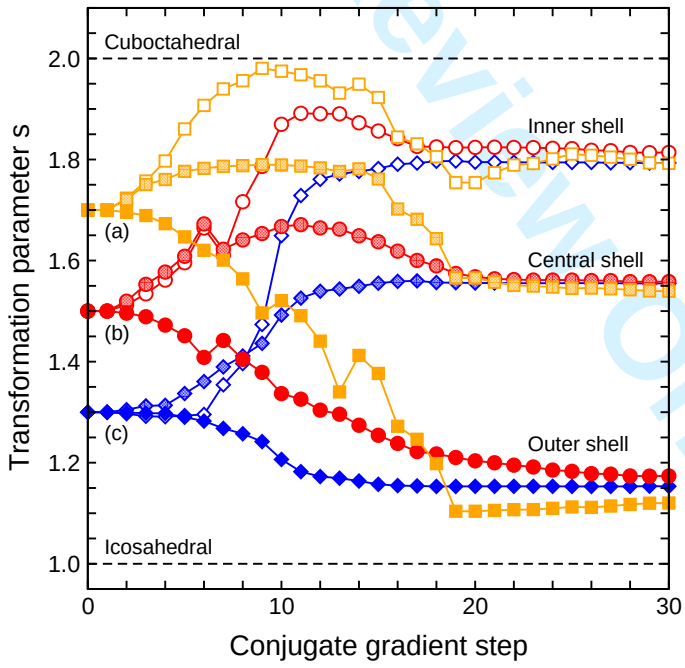

Figure 2. Evolution of the shell-wise decomposed degree of transformation of three differently initialized Fe_{147} isomers (a), (b), and (c) observed in *ab initio* conjugate gradient optimization runs. The initial morphologies are homogeneously transformed along the Mackay-path, but different degrees 1.3, $s = 1.5$ and $s = 1.7$ (for all shells) for (a), (b) and (c), respectively. The three isomers are represented by the shape of the symbols (squares, circles and diamonds, respectively), while open symbols denote to the innermost shell, filled symbols the outermost and shaded ones the central shell of the respective isomer.

of the Fe atoms near the outer shells [13]. This clearly demonstrates the influence of magnetism on the structure of Fe nanoclusters. If the number of shells n exceeds a critical value then the SMT clusters are no longer stable but transform entirely to the bcc structure [32]. This happens for $n > 15$ where n is the number of complete atomic shells of the cluster, which yields $N = \frac{1}{3}(10n^3 + 15n^2 + 11n + 3)$ for the number of atoms in perfect icosahedra as well as fcc cuboctahedra.

The evolution of the energy landscape for different isomers as a function of the cluster size for iron nanoclusters with complete atomic shells is shown in Fig. 3, showing that the SMT structure is preferred over the icosahedral and cuboctahedral forms while the bcc transformed cuboctahedron becomes lowest in energy for clusters with number of atoms larger than 147. Of further interest is the variation of the average cluster magnetic moment with the cluster size obtained from the *ab initio* calculations compared to the experimental results of Billas at a fixed temperature of 120 K [19, 29, 30]. It is shown in [13] that the zero-temperature calculations are accurate enough to reproduce the variation of the average magnetic moment with cluster size as observed in experiment [13, 33].

3. Collinear versus non-collinear spin moments in monometallic Fe clusters

The tendency of forming non-collinear magnetic moments in monometallic Fe and in some bimetallic transition metal clusters has been studied using density functional theory [25, 34, 35]. There are two observations. First, allowing only for collinear magnetic structures in the monometallic Fe nanoclusters in Sec. 2, we find that for all isomers besides those with bcc geometry, the magnetic structure is of core-shell type meaning that there is a shellwise antiferromagnetic core while usually the two outermost shells are ferromagnetic. Second, when allowing for non-collinear magnetic ordering, the situation becomes rather complex since the role of morphology of the cluster, electronic correlation, spin-orbit interaction and the energetic behavior of the cluster with varying spin multiplicity needs to be discussed.

For example, for a tiny cluster like Fe_5 the energetic and magnetic relationships between local minima on the potential surface can be found in [25]: Here, the perfect trigonal bipyramid with non-collinear magnetic moments is lower in energy than the corresponding cluster with collinear magnetic moments. However, when relaxing the atomic

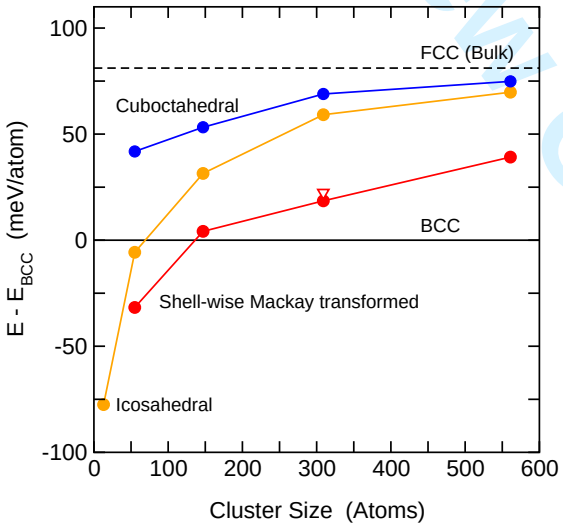

Figure 3. *Ab initio* total energy of optimized (relaxed) Fe nanoclusters with complete atomic shells showing that the Mackay transformed iron clusters are favored with respect to the other isomers. Reference energy for each cluster size is the bcc cluster (which corresponds to the Bain transformed cuboctahedron) which is lowest in energy for cluster sizes larger than Fe_{147}. Data originally published in [13], copyright (2007) by the American Physical Society.

positions the resulting structure is Jahn-Teller distorted and shows a collinear spin structure. When adding electronic correlations using the GGA + U method, in general collinear magnetism is favored. When switching on spin-orbit interaction, the magnetic moments become non-collinear, however, in many cases the non-collinearity is a small effect. This has been checked for the Fe_{13}, Co_{13} and Ni_{13} clusters for which larger deviations from collinearity can be achieved by decorating the clusters with other magnetic atoms [35]. The orbital and spin magnetic moments as well as the magnetic anisotropy energy as function of the rotation angle of the magnetic moment can be found in [35]. These investigations show systematic differences of spin and orbital magnetic moments as compared to corresponding bulk values, in particular the magnetic anisotropy energy of the clusters is orders of magnitude larger than the bulk values. For details, see [35]. Altogether, the calculations show that further investigations of non-collinear tendencies are required especially of what concerns the larger transition metal clusters for which we find *magnetic core-shell configurations*.

Since *magnetic core-shell configurations* reminds one of the discussion of of low- and high-spin states in bulk fcc Fe and Fe-Ni [36], it is interesting to look a bit closer at the dependence of energy on spin multiplicity for the smaller clusters. This is under current investigations, here we cite some preliminary results obtained for icosahedral Fe, Co, Ni and FeNi and CoNi clusters [37]. For exampel, Fig. 4 shows how the total energy of the icosahedral structures of Fe_{13} and Co_{13} depends on the total spin moment for each cluster, which was fixed for each run using the fixed spin moment method [38]. In these calculation all spins have been kept collinear. For Co_{13}, there is some qualitative agreement with previous calculations based on the discrete variational $X\alpha$ method [39].

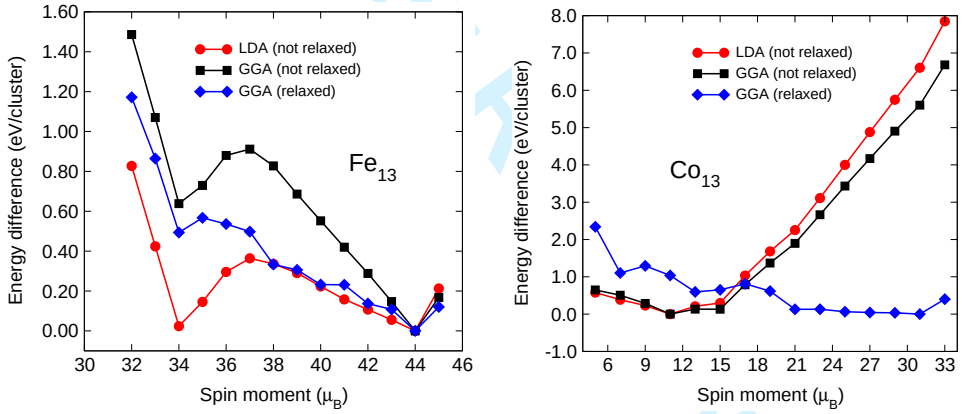

Figure 4. Total energy of icosahedral Fe_{13} (left) and Co_{13} (right) as a function of the spin moment obtained by fixed spin moment calculations. For each curve, the corresponding lowest energy state has been chosen as energy reference, which for Fe_{13} is the high-spin state with 44 μ_B/cluster (irrespective of whether the local density approximation (LDA) or the generalized gradient approximation (GGA) is used), the low-spin state of Fe_{13} with 34 μ_B/cluster and a reversed central spin is higher in energy. For Co_{13}, we find several local minima, the lowest in energy using GGA and relaxed structure is again the high spin state (31 μ_B/cluster). The figures show that it is essential to take relaxation of the atomic position into account.

4. Bimetallic (Fe, Co)Pt clusters

Bimetallic FePt and CoPt nanoclusters have been subject of intense experimental [40–48] as well as theoretical [14, 49–56] investigations, in particular because of their potential use in miniaturized storage media requiring monodisperse FePt nanoparticles and ferromagnetic FePt nanocrystal superlattices [57–59] and in nanocatalysis where the catalytic properties of highly dispersed supported bimetallics are used [60, 61].

The interest in FePt nanoclusters for applications in perpendicular magnetic recording is associated with the high magnetocrystalline anisotropy of the corresponding bulk ma-

terial in the layered $L1_0$ structure with a c/a distortion of about 0.97 around $Fe_{50}Pt_{50}$ [59, 62], see Fig. 6. The best quality nanoparticles with a diameter of ~ 5 nm can be used to obtain self-organized FM arrays of dispersed $L1_0$ particles. However, the coercivity field, which can be achieved, is still an order of magnitude lower than corresponding $L1_0$ bulk material [42, 63]. Figure 5 shows coercivity data of $Fe_{62}Pt_{38}$ taken from hysteresis curves of the magnetization for different particle sizes, which have been extrapolated to zero temperature. At room temperature and for diameters lower than 6-7 nm, the coercivity field drops to vanishingly small values due to surface effects and associated twin boundary formation or appearance of multiply twinned structures in the particles. This has been checked by *ab initio* calculations for FePt nanoclusters with a diameter of the order of 2.5 nm showing that the multiply twinned clusters are lower in energy than the $L1_0$ clusters [14]. Therefore, the interest in trimetallic FePt-X clusters where the third element may be chosen to favor the $L1_0$ formation. There is no ultimate solution so far, molecular dynamics simulations seem to show that X = Ag or Au may be a proper choice since they allow to reduce the annealing temperature by 100-150°C [64], as these elements are expected to support ordering kinetics due to their strong demixing tendencies of their Fe-alloys. Other experiments aim at inserting nitrogen into the particles in the gas phase so that $L1_0$ more easily forms due to atomic diffusion at elevated temperatures. Accompanying *ab initio* simulations have still to be done. The difficulty to achieve the $L1_0$ structure for the smaller cluster sizes (below 3 nm) becomes obvious if one compares the energetic evolution of different isomers of the bimetallic nanoclusters as shown in Fig. 7. The calculations of the bimetallic FePt clusters have been carried on the Blue Gene/L in Jülich, which have meanwhile been continued on the Blue Gene/P up to a cluster size of roughly 3 nm corresponding to a total number of atoms of 923 [65]. The trend shown in Fig. 7 continues up this cluster size: The icosahedron with alternating Fe/Pt shells (c) remains lower in energy than the $L1_0$-orderd cuboctahedron (a).

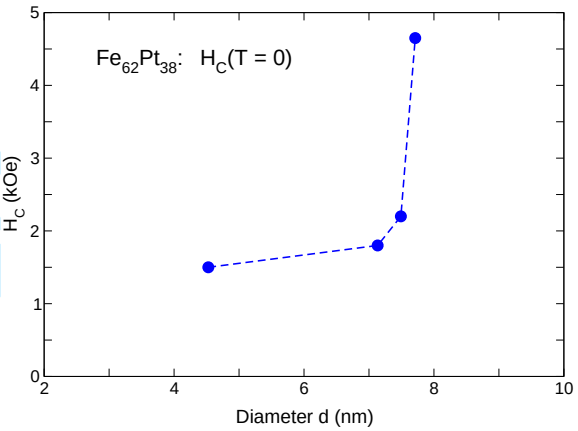

Figure 5. Coercivity fields as a function of the size of the $Fe_{62}Pt_{38}$ clusters. The data have been extrapolated to zero temperature from the room temperature measurements of the hysteresis curves. Figure adapted from [42].

Similar calculations have been performed for other bimetallic clusters of interest like CoPt and FePd [14, 66], All calculations done so far for bimetallic clusters energetically favor other morphologies and that the $L1_0$ isomer is in none of the cases lowest in energy. In case of CoPt, the segregation tendency of Pt atoms to the surface of the nanoclusters is more pronounced than for the FePt clusters. The rather strong segregation of Pt in CoPt clusters has experimentally been confirmed and modelled by performing Monte Carlo simulations [67]. However, there is a recent interesting attempt to obtain 3 nm large CoPt clusters in the $L1_0$ structure by making samples of diluted layers of CoPt clusters embedded in amorphous carbon. This seems to favor the formation of the $L1_0$ geometry and may be a promising route to get the desired $L1_0$ structure with large magentocrys-

talline anisotropy [68]. The (Fe, Co) clusters considered in this paper are all free clusters, embedding the clusters would require *ab initio* calculations on an even larger scale.

5. Collinear versus non-collinear spin moments in bimetallic (Fe, Co)Pt clusters

Regardless of the morphology, the spin moments of Fe or Co and induced spin moments of Pt of (Fe, Co)Pt have all been taken to be collinear in the calculations. In contrast to the monometallic Fe clusters. we observe no tendency for the reversal of spin moments in the inner shells of the (Fe, Co)Pt nanoclusters. Figure 8 shows the average magnetic moment per atom of various morphologies as a function of the cluster size. The calculations of smaller transition metal clusters capped with Pt atoms show the existence of non-collinear spin configurations, however, for the larger (Fe, Co)Pt clusters we have not observed strong non-collinear trends. However, further calculations are needed like, for instance, a continuation of *ab initio* calculations to finite temperatures by using an effective Heisenberg-like spin Hamiltonian.

6. Trimetallic (Ni, Co)MnGa clusters

First-principles calculations of the full Heusler alloys have shown an extreme variation of the physical properties with small changes of the composition [9, 69]. Even the magnetocaloric and inverse magnetocaloric effect can be observed in one and the same sample with varying temperature [10]. One important ingredient for occurrence of the magnetocaloric effect in the FM Heusler alloys is the coexistence of the magnetic phase transition and the martensitic phase transformation (magnetostructural phase transition) over a substantial range of composition, temperature, magnetic field and external pressure. For instance, such a coupled magnetostructural phase transition exists in Ni-Mn-Ga at larger Ni excess concentrations shown in Fig. 9 where the magnetic and structural phase transition lines merge in the interval $0.22 < x < 0.27$ [70]. Note that the magnetocaloric effect especially in the Heuslers Ni_2MnZ (Z = In, Sn, Sb) is connected with the observation of competing FM and AFM interactions leading to metamagnetic effects at temperatures below the martensitic transformation [71].

In most experiments, polycrystalline samples are used because of the difficulty to grow

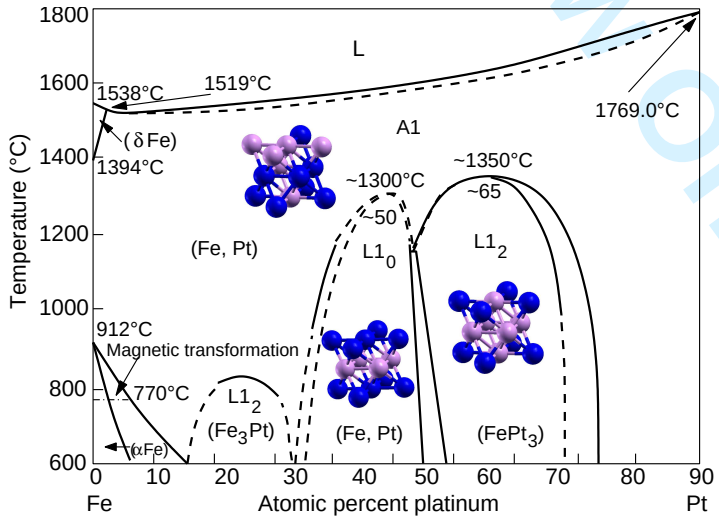

Figure 6. Equilibrium phase diagram and crystallographic structures of FePt with the $L1_0$ structure around 50 at.% Fe. The magnetic properties of thin films, nanocrystalline materials and nanoparticles differ depending on the approach used to achieve the $L1_0$ phase. Figure adapted from [59, 62].

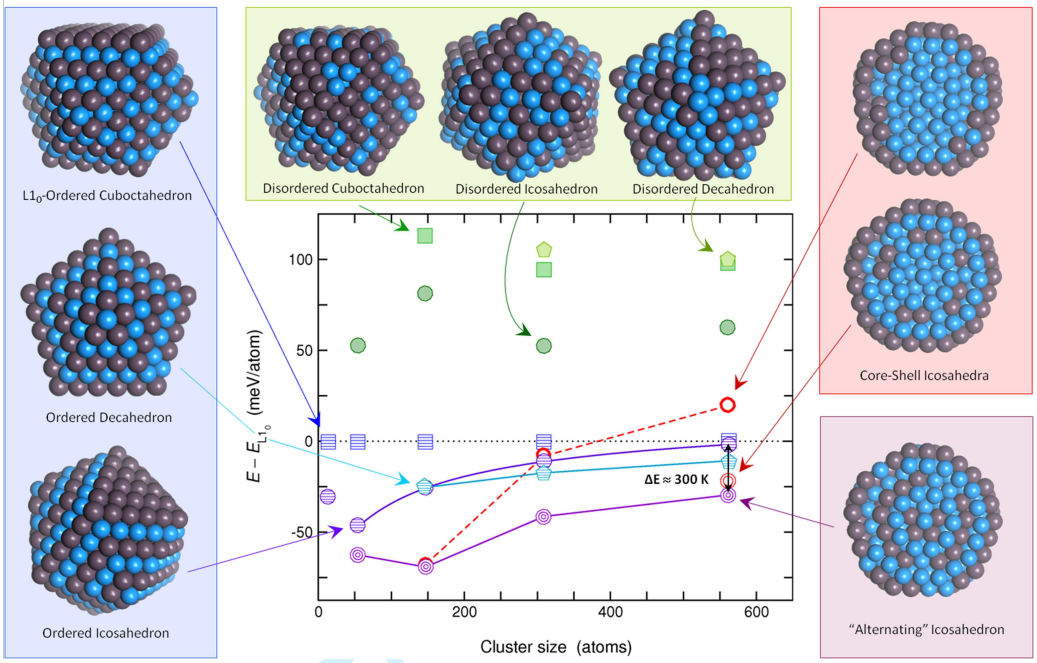

Figure 7. *Ab initio* energies of different morphologies of FePt nanoclusters as a function of the cluster size. All clusters have been relaxed during the calculations. For each cluster size the energy reference is defined by the $L1_0$ cuboctahedron (upper left). Only the structures with $N = 561$ atoms (265 Fe and 296 Pt) are depicted in (for clarity the arrow for each morphology is directed to its corresponding symbol). Blue spheres refer to Fe atoms, brown spheres to Pt. The icosahedral structures on the right are shown as cross sections. The figure illustrates that the disordered structures are energetically unfavorable while ordered core-shell structures or the icosahedron with alternating Fe/Pt shells are energetically favored over the $L1_0$ structure. Data originally published in [14], copyright (2008) by the American Physical Society.

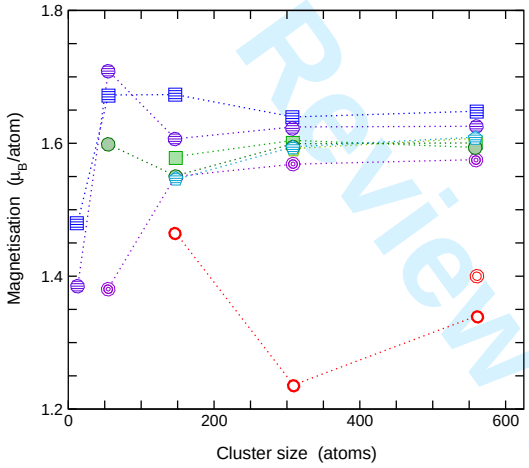

Figure 8. Average magnetic moment per atom of various FePt morphologies as a function of the cluster size. The symbols are the same as in Fig. 7. Data originally published in [14], copyright (2008) by the American Physical Society.

single crystals. Therefore, it is an intriguing question in how far are the technologically relevant properties of bulk Heuslers survive if one uses nanocrystalline materials instead which may be easier to grow. We have performed a few preliminary investigations of free Heusler clusters. The main observation is that for the smaller clusters the magnetic properties may drastically change due to the magnetic contributions from the surface atoms. Figure 10 highlights the energy landscape of cubic-like trimetallic Ni-Mn-Ga Heusler clusters showing that the structures closest to stoichiometry have lowest energies [18]. Clusters were prepared by cutting spherical forms of specific radii from bulk $L2_1$ Ni_2MnGa (mostly with a Ga atom at the center of the cut fragment). For the energetically favorable clusters with $N = 65,\ 169$ atoms we have compositions $Ni_{32}Mn_{14}Ga_{19}$ [$Ni_{1.97}Mn_{0.86}Ga_{1.16}$] and $Ni_{88}Mn_{38}Ga_{43}$ [$Ni_{2.083}Mn_{0.9}Ga_{1.917}$] for

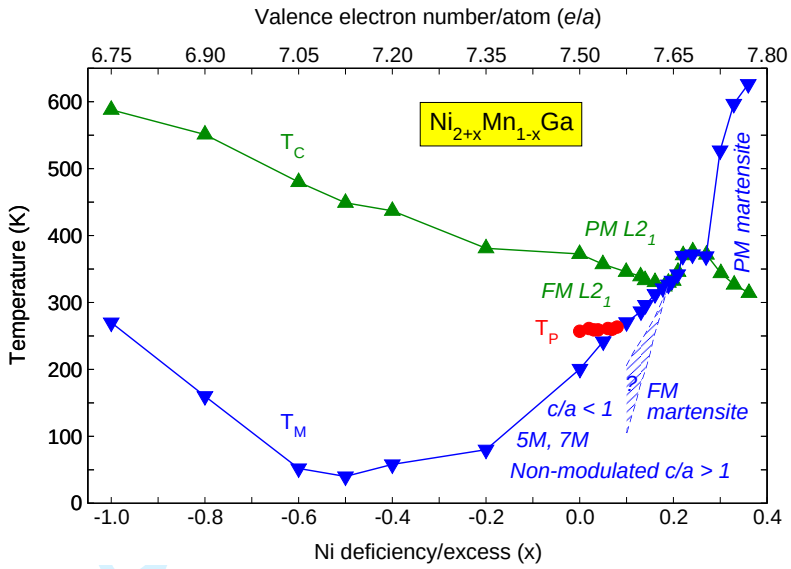

Figure 9. Phase diagram of $Ni_{2\pm x}Mn_{1-\pm x}Ga$ as a function of either Ni deficiency or Ni excess concentration. PM and FM $L2_1$ denote the cubic paramagnetic and ferromagnetic phases, respectively, 5M and /M denote the tetragonal phases with $c/a = 0.94$. For Ni excess concentration Larger than 0.1, there is a gradual transition for modulated to non-modulated phases with $c/a \sim 1.25$. A magnetostructural phase transition occurs for $0.22 < x < 0.27$. Figure adapted from data available in the literature, mainly from [70].

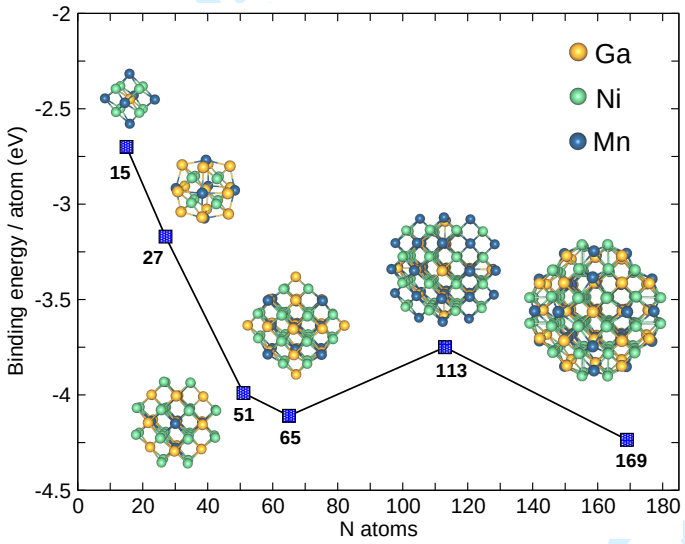

Figure 10. Energy landscape of cubic-like trimetallic Ni-Mn-Ga Heusler clusters showing that the structures which are closest to stoichiometry ($N = 65,\ 169$ atoms) have lowest energies. Calculations have been done with the PARSEC code [16]. The binding energy per atom has been obtained by subtracting the sum of elemental energies of isolated atoms from the total energies of the relaxed clusters. Figure adapted from [18].

which the corresponding bulk materials exhibit the magnetic shape memory effect [9]. Stress versus strain curves in an external magnetic field or energy versus c/a variation need to be calculated for the individual clusters in order to see in how far the magnetic shape memory effect may be a typical property of Heusler clusters too. This is under current investigation.

We have also calculated Heusler clusters cut from bulk Co_2MnGa which is of interest for spin injection devices because of its half-metallic character and 100% spin polarization in the majority-spin channel. It seems that for these cluster the 100% spin polarization is reduced to due the surface with reversed spin moments, see [17].

7. Collinear versus non-collinear spin moments in trimetallic clusters (Ni, Co)MnGa

Magnetism in ternary bulk systems like Ni_2Mn(Ga, In, Sn, Sb) is mainly determined by the interaction of the Ni and Mn spin moments on different sublattices [74]. A close look at the related binary systems like $L1_0$ NiMn (which is AFM) [72], $L1_2$ Ni_3Mn (where ordered Ni_3Mn is strongly ferromagentic while disordered Ni_3Mn is only paramagnetic) [73], and $L2_1$ Ni_3Ga (being a strongly exchange-enhanced paramagnet) at least helps to understand trends of the magnetic properties of the ternary systems like the strong admixture of AFM interactions when partially replacing Ga by In, Sn or Sb. When making films of nanoclusters mixtures of different structures occur and the magnetic order seems mostly to be determined by short-range magnetic order [76]. A systematic search for the cluster properties of Ni_2Mn(Ga, In, Sn, Sb) covering compositions for which the shape-memory effect should be visible, and other compositions for which magnetocaloric effect may be expected, has yet to be undertaken. We expect for the alloy clusters coexisting FM and AFM interactions and a strong tendency for non-collinear spin moments of the Mn atoms.

8. Conclusions

Multimetallic transition metal clusters show intriguing properties, the richness of which still needs to be explored in more details by further first-principles calculations and experiments. For the mono- and bimetallic Fe and FePt clusters, we have limited the discussion to clusters with closed atomic shells in order not to meet the necessity to discuss properties for all kind of morphologies. Here, we have seen that shellwise Mackay transformed cluster can be understood by ferromagnetism influencing the cluster formation. The richness of Heusler clusters still requires further investigations.

Acknowledgment

One of us (P.E.) would like to thank Peter Weinberger for the hospitality and the extremely nice workshop held in Cocoyoc, Mexico, in February 2008. Financial support was granted by the Deutsche Forschungsgemeinschaft (SFB 445 and SPP 1239). We thank the staff of the John von Neumann Institute for Computing for substantial support of our project *Nanometer-scale ab initio investigations of functional magnetic materials*.

References

[1] D. Sellmeyer and R. Skomski (eds.), *Advanced Magnetic Nanostructures*, Springer, New York, NY, 2006.
[2] S.A. Wolf, D.D. Awschalom, R.A. Buhrman, J.M. Daughton, S. von Molnár, M.L. Roukes, A.Y. Chtchelkanova, and D.M. Treger, Science 294 (2001), p. 1488.
[3] Review: R. Ramesh, and N.A. Spaldin, Nature Mater. 6 (2007), p. 21.
[4] S. Gangopadhyay, G.C. Hadjipanayis, C.M. Sorensen, and K.J. Klabunde, J. Appl. Phys. 73 (1993), p. 6964.
[5] Review: J. Nogués and I.K. Schuller, J. Magn. Magn. Mater. 192 (1999), p. 203.
[6] J. Sinova, D. Culcer, Q. Niu, N.A. Sinitsyn, T. Jungwirth, and A. Macdonald, Phys. Rev. Lett. 92 (2004), p. 126603.
[7] Review: L.D. Pachón and G. Rothenberg, Appl. Organometallic Chem. 22 (2008), p. 288.
[8] J. Li, M. Mirzamaani, X. Bian, M. Doerner, S. Duan, K. Tang, M. Toney, T. Arnoldussen, and M. Madison, J. Appl. Phys. 85 (1999), p. 4286.
[9] Review: P. Entel, V.D. Buchelnikov, V.V. Khovailo, A.T. Zayak, W.A. Adeagbo, M.E. Gruner, H.C. Herper, and E.F. Wassermann, J. Phys. D: Appl. Phys. 39 (2006), p. 865.
[10] T. Krenke, E. Duman, M. Acet, E.F. Wassermann, X. Moya, L. Mañosa, and A. Planes, Nature Mater. 4 (2005), p. 450.
[11] G. Kresse and J. Furthmüller, Phys. Rev. B 54 (1996), p.11169.
[12] G. Kresse and D. Joubert, Phys. Rev. B 59 (1999), p. 1758.
[13] G. Rollmann, M.E. Gruner, A. Hucht, R. Meyer, P. Entel, M.L. Tiago, and J.R. Chelikowsky, Phys. Rev. Lett. 99 (2007), p. 083402.
[14] M.E. Gruner, G. Rollmann, P. Entel, and M. Farle, Phys. Rev. Lett. 100 (2008), p. 087203.

[15] M.E. Gruner, J. Phys. D: Appl. Phys. (2008), in print.
[16] J.R. Chelikowsky, N. Troullier, and Y. Saad, Phys. Rev. Lett. 72 (1994), p. 1240, see http://www.ices.utexas.edu/parsec/.
[17] A.T. Zayak, P. Entel, and J.R. Chelikowsky, Phys. Rev. B (2008), in print.
[18] A.T. Zayak, S.P. Beckman, M.L. Tiago, P. Entel, and J.R. Chelikowsky, submitted to J. Appl. Phys.
[19] I.M.L. Billas, A. Châtelain, and W.A. de Heer, J. Magn. Magn. Mater. 168 (1997), p. 64.
[20] Y. Xing, T.P. Kole, and J.L. Katz, J. Mater. Sci. Lett. 22 (2004), p. 787.
[21] J, Knipping, H. Wiggers, B.F. Kock, T. Hülser, B. Rellinghaus, and P. Roth, Nanotechn. 15 (2004), p. 1665.
[22] Review: D.L. Huber, Small 5 (2005), p.482.
[23] T.P. Huelser, H. Wiggers, P. Ifeacho. O. Dimitrieva, and G. Dumpich, Nanotechn. 17 (2006), p. 3111.
[24] Review: J.A. Alonso, Chem. Rev. 100 (2000), p. 637.
[25] G. Rollmann, P. Entel, and S. Sahoo, Comput. Mater. Sci. 35 (2006), p. 275.
[26] A. Hucht, S. Buschmann, and P. Entel, Europ. Phys. Lett. 77 (2007), p. 57003.
[27] A.L. Mackay, Acta Crystallogr. 15 (1962), p. 916.
[28] E.C. Bain, Trans. Am. Inst. Min. Metall. Pet. Eng. 70 (1924), p. 25.
[29] I.M.L. Billas, J. A. Becker, A. Châtelain, and W.A. de Heer, Phys. Rev. Lett. 71 (1993), p. 4067.
[30] I.M.L. Billas, J. A. Becker, and W.A. de Heer, Science 265 (1994), p. 1682.
[31] D. Faken and H. Jónsson, Comput. Mater. Sci. 2 (1994), p. 279.
[32] A. Hucht, R. Meyer, and P. Entel, in preparation.
[33] M. Tiago, Y. Zhou, M.M.G. Alemany, Y. Saad, and J.R. Chelikowsky, Phys. Rev. Lett. 97 (2006), p. 147201.
[34] G. Rollmann and P. Entel, Comput. Lett. 1 (2004), p. 288.
[35] S. Sahoo, P. Entel, A. Postnikov, and M. Richter, submitted to Phys. Rev. B.
[36] E.F. Wassermann, *Invar: Moment-Volume Instabilities in Transition Metals and Alloys*, in *Handbook of Ferromagnetic Materials*, K.H.J. Buschow and E.P. Wohlfarth (eds.), Vol. 5, Amsterdam, Elsevier, 1990, p. 237.
[37] S. Sahoo, in preparation.
[38] V.L. Moruzzi, P.M. Marcus, K. Schwarz, and P. Mohn, Phys. Rev. B 34 (1986), p. 1784.
[39] K. Miura, H. Kimura, and S. Imanaga, Phys. Rev. B 50 (1994), p. 10335.
[40] Z.R. Dai, S. Sun, and Z.L. Wang, Surf. Sci. 505 (2002), p. 325.
[41] S. Stappert, B. Rellinghaus, M. Acet, and E.F. Wassermann, J. Cryst. Grwoth 252 (2003), p. 440.
[42] B. Rellinghaus, S. Stappert, M. Acet, and E.F. Wassermann, J. Magn, Magn, Mater. 266 (2003), p. 142.
[43] J. Lyubina, I. Opahle, K.-H. Müller, O. Gutfleisch, M. Richter, M. Wolf, and L. Schultz, J. Phys.: Condens. Matter 17 (2005), p. 4157.
[44] O. Dimitrieva, M. Acet, G. Dumpich, J. Kästner, C. Antoniak, M. Farle, and K. Fauth, J. Phys. D: Appl. Phys. 39 (2006), p. 4741.
[45] C. Antoniak, J. Lindner, M. Spasova, D. Sudfeld, M. Acet, M. Farle, K. Fauth, U. Wiedwald, H.-G- Boyen, and P. Ziemann, Phys. Rev. Lett. 97 (2006), p. 117201.
[46] O. Dmitrieva, M. Spasova, C. Antoniak, M. Acet, G. Dumpich, J. Kästner, M. Farle, K. Fauth, U. Wiedwald, H.-G. Boyen, and P. Ziemann, Phys. Rev. B 76 (2007), p. 064414.
[47] R. M. Wang, O. Dmitrieva, M. Farle, G. Dumpich, H.Q. Ye, H. Poppa, R. Kilaas, and C. Kisielowski, Phys. Rev. Lett. 100 (2008), p. 017205.
[48] J. Penuelas, P. Andreazza, C. Andreazza-Vignolle, H.C.N. Tolentino, M. De Santis, and C. Mottet, Phys. Rev. Lett. 100 (2008) 115502.
[49] N. Lümmen and T. Kraska, Phys. Rev. B 77 (2008), p. 045425.
[50] N. Lümmen and T. Kraska, Eur. Phys. J. D 41 (2007), p. 247.
[51] G. Rossi, R. Ferrando, and C. Mottet, Faraday Discuss. 138 (2008), p. 193.
[52] M. Müller, P. Erhart, and K. Albe, Phys. Rev. B 76 (2007), p. 155412 (2007).
[53] M. Müller and K. Albe, Acta Mater. 55 (2007), p. 6617.
[54] M. Müller and K. Albe, Phys. Rev. B 72 (2005), p. 094203.
[55] D. Cheng, S. Huang, and W.Wang, Cem. Phys. 330 (2006), p. 423.
[56] Y.H. Chui and K.-Y. Chan, Molec. Simul. 30, 679 (2004), p. 679.
[57] S. Sun, C.B. Murray, D. Weller, L. Folks, and A. Moser, Science 287 (2003), p. 1989.
[58] D. Sellmyer, M. Yan, Y. Xu, and R. Skomski, IEEE Trans. Magn. 41 (2005), p. 560
[59] O. Gutfleisch, J. Lyubina, K.-H. Müller, and L. Schultz,, Adv. Eng. Mater. 7 (2005), p. 208.
[60] J. Luo, L. Wang, D. Mott, P.N. Njoki, N. Kariuki, C.J. Zhong, and T. He, J. Mater. Chem. 16, (2006), p. 1665.
[61] O.S. Alexeev and B.C. Gates, In. Eng. Chem. Res. 42 (2003), p. 1571.
[62] T.B. Massalski (ed.), *Binary Alloy Phase Diagrams*, Ohio, ASM Interantional, 1990, p. 1752.
[63] U. Wiedwald, unpublished data.
[64] I. Zafiropoulou, V. Tzitzios, N.Boukos, and D. Niarchos, J. Magn, Magn. Mater. 316 (2007), p. e169.
[65] M.E. Gruner, unpublished data.
[66] M.E. Gruner and A. Dannenberg, submitted to J. Magn. Magn. Mater.
[67] S. Heinrichs, W. Dieterich, and P. Maass, Europhys. Lett. 75 (2006), p. 167.
[68] F. Tournus, A. Tamion, N. Blanc, A. Hannour, L. Bardotti, B. Prével, P. Ohresser, E. Bonet, T. Epicier, and V. Dupuis, Phys, Rev. B 77 (2008), p. 144411.
[69] P. Entel, V.D. Buchelnikov, M.E. Gruner, A. Hucht, V.V. Khovailo, S.K. Nayak, A.T. Zayak, Mater. Sci. Forum 583 (2008), p. 21.
[70] V.V. Khovaylo, V.D. Buchelnikov, R. Kainuma, V.V.Koledov, M. Ohtsuka, V.G. Shavrov, T. Takagi, S.V. Taskaev, and A.N.Vasiliev, Phys. Rev. B 72 (2005), p. 224408; V.V. Khovaylo, unpublished.
[71] V.D. Buchelnikov, S.V. Taskaev, M.A. Zagrebin, and P. Entel, Mater. Sci. Forum 583 (2008), p. 131.
[74] J. Kübler, *Theory of itinerant Electron Magnetism*, Oxford, Clarendon Press, 2000.
[72] K. Nakamura, M. Kim, A.J.Freeman, L. Zhong, and J. Fernandez-de-Castro, IEEE Trans. Magn. 36 (2000), p. 3269.
[73] T. Nautiyal and S. Auluck, Phys. Rev. B (1993), p. 12921.
[75] S.M. Hayden, G.G. Lonzarich, and H.L. Skriver, Phys. Rev. B 33 (1986), p. 4977.
[76] A.J. Garcia-Adeva, R.C. Howell, S.D. Conradson, J.F. Mustre de Leon, and F.J. Espinosa-Faller, J. Phys. Chem. 109 (2005), p. 10419.

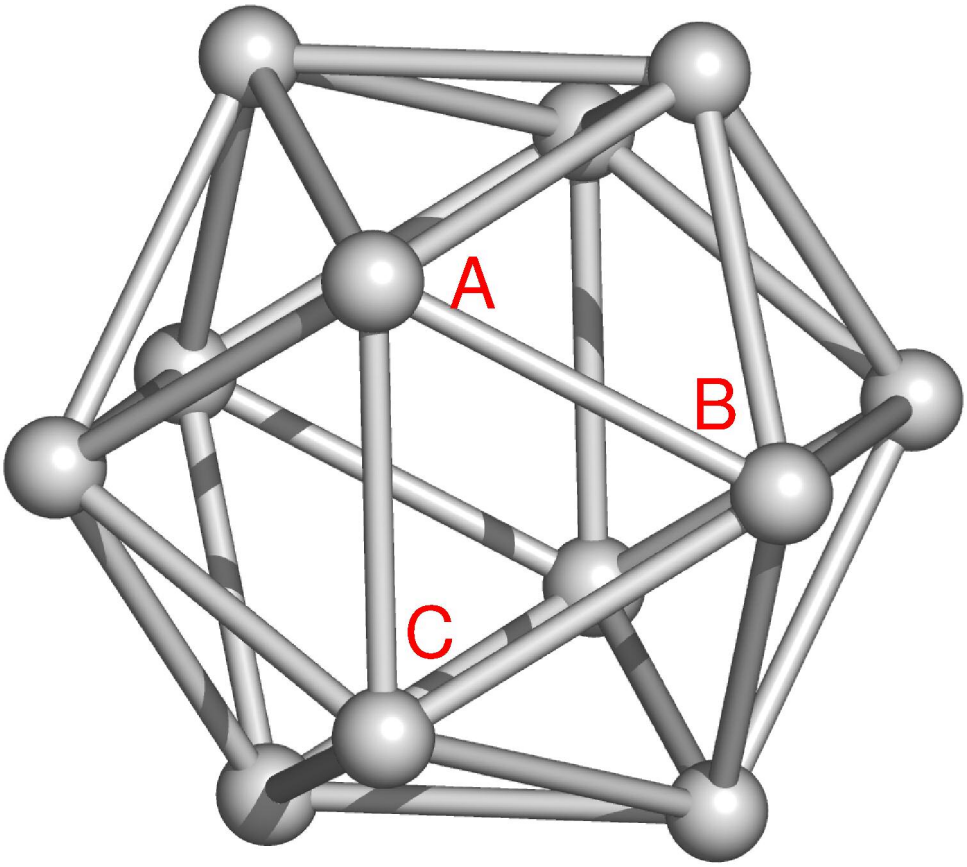

353x316mm (600 x 600 DPI)

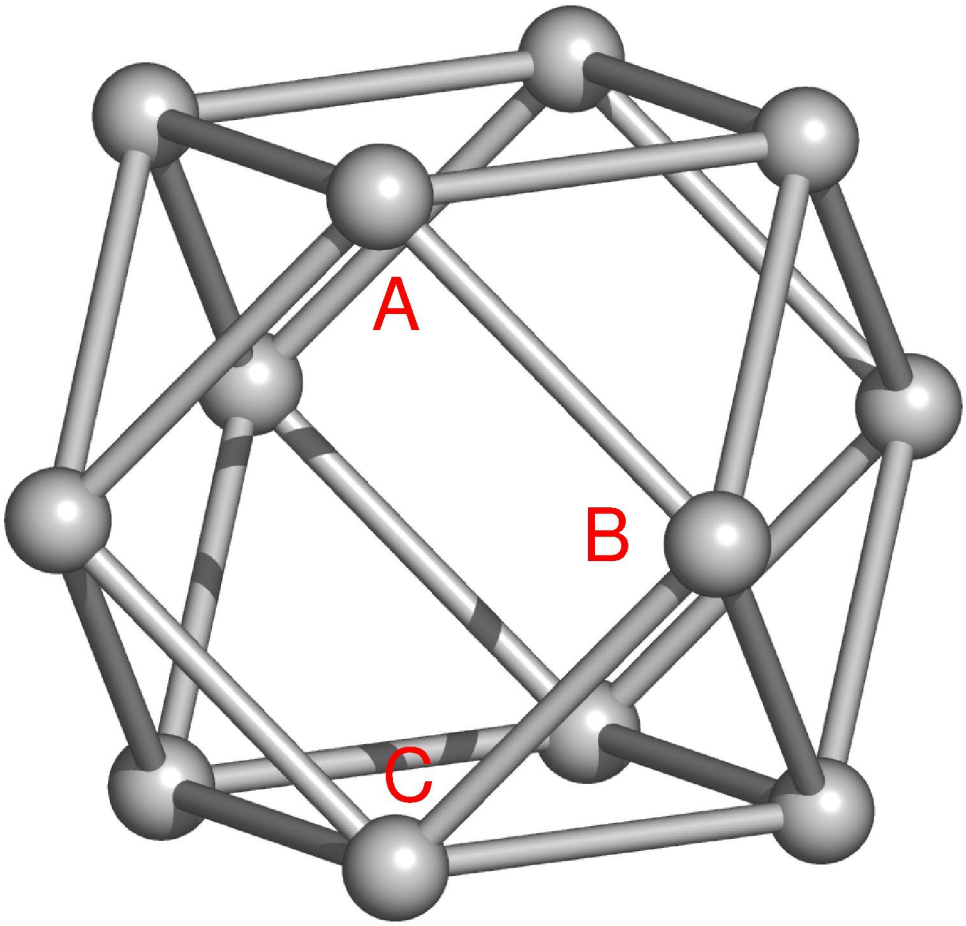

340x323mm (600 x 600 DPI)

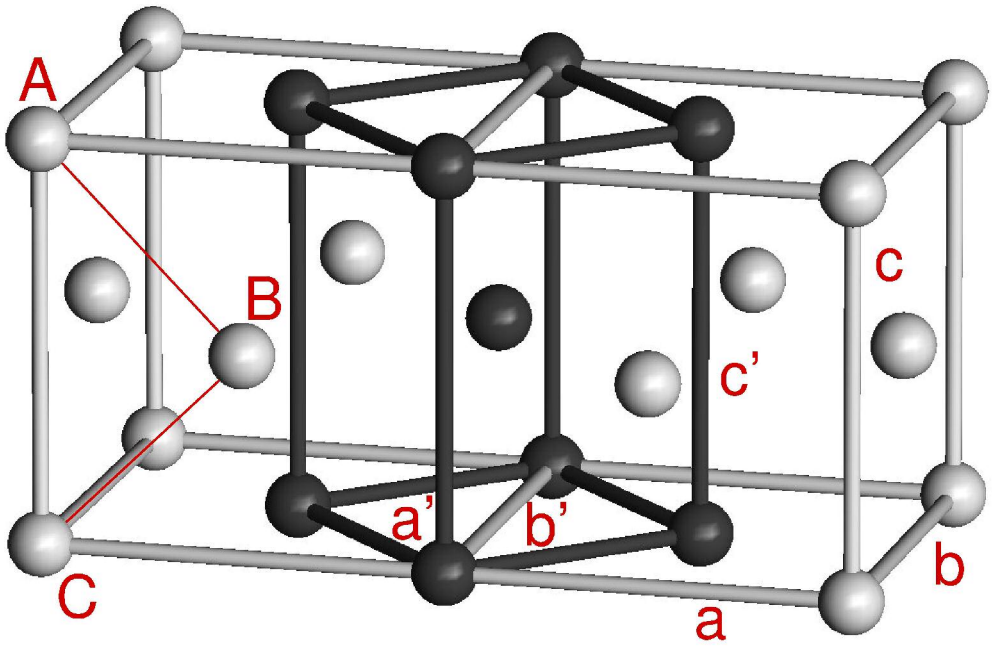

157x101mm (600 x 600 DPI)

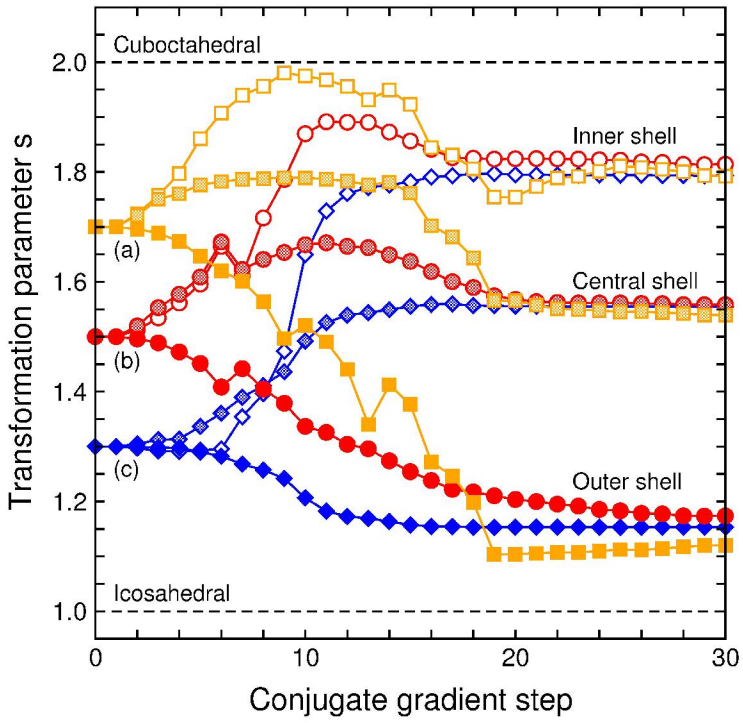

215x279mm (600 x 600 DPI)

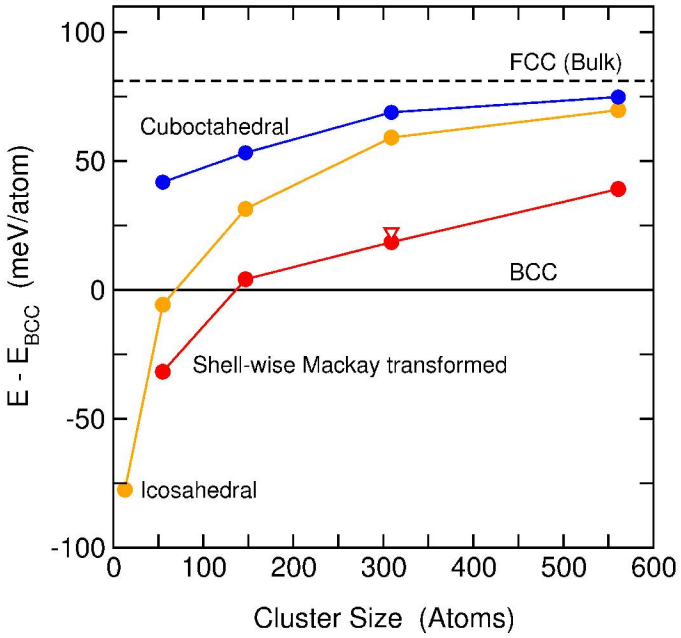

215x279mm (600 x 600 DPI)

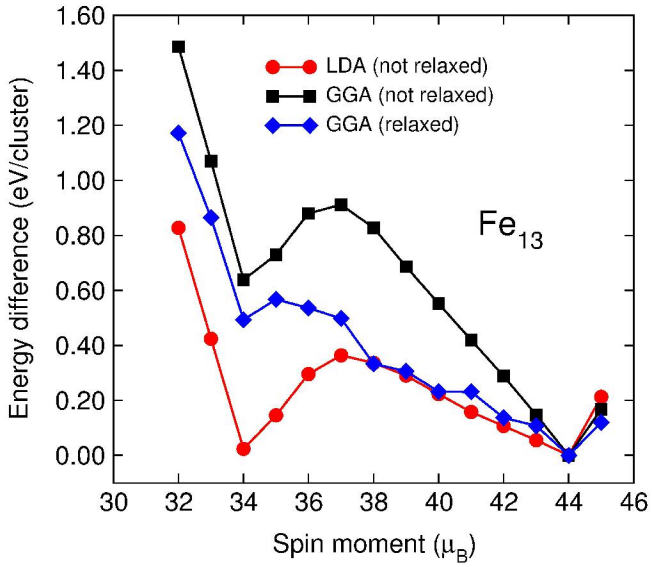

215x279mm (600 x 600 DPI)

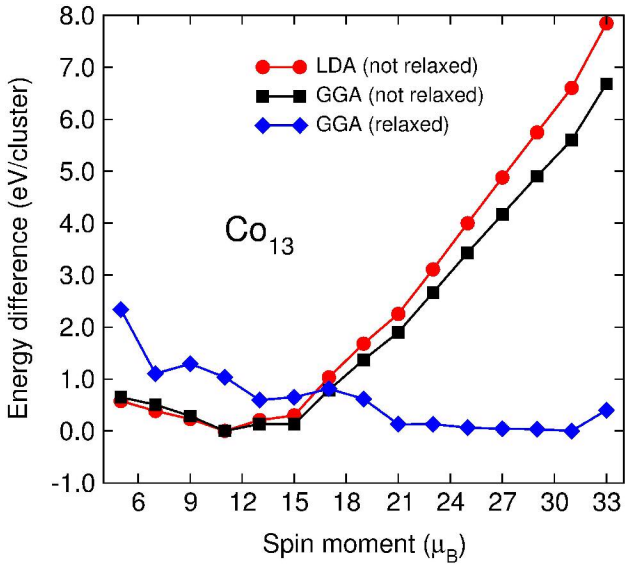

215x279mm (600 x 600 DPI)

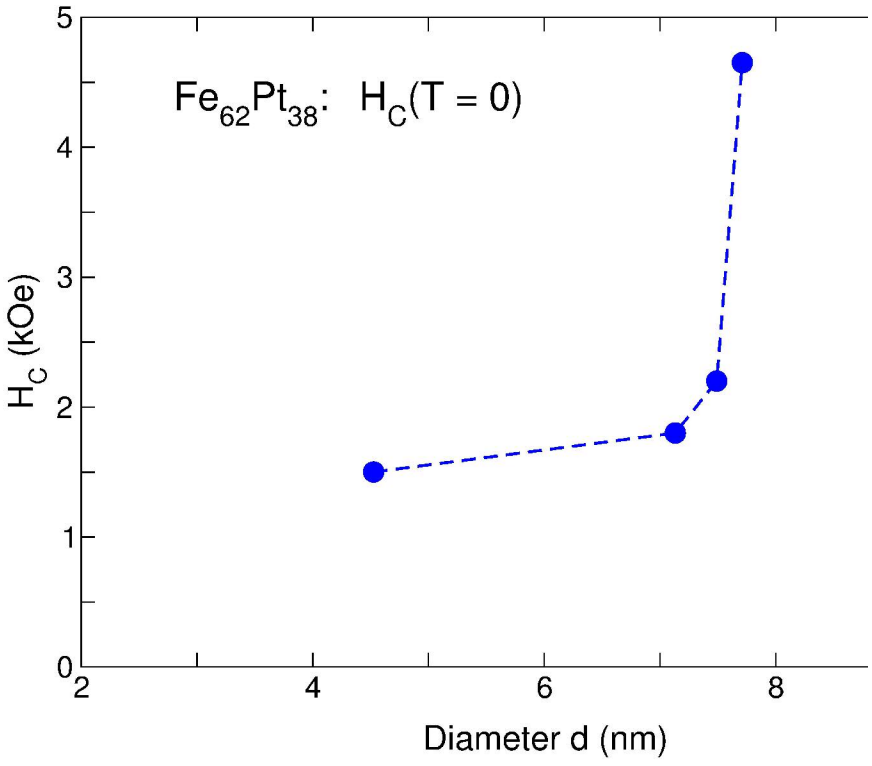

215x279mm (600 x 600 DPI)

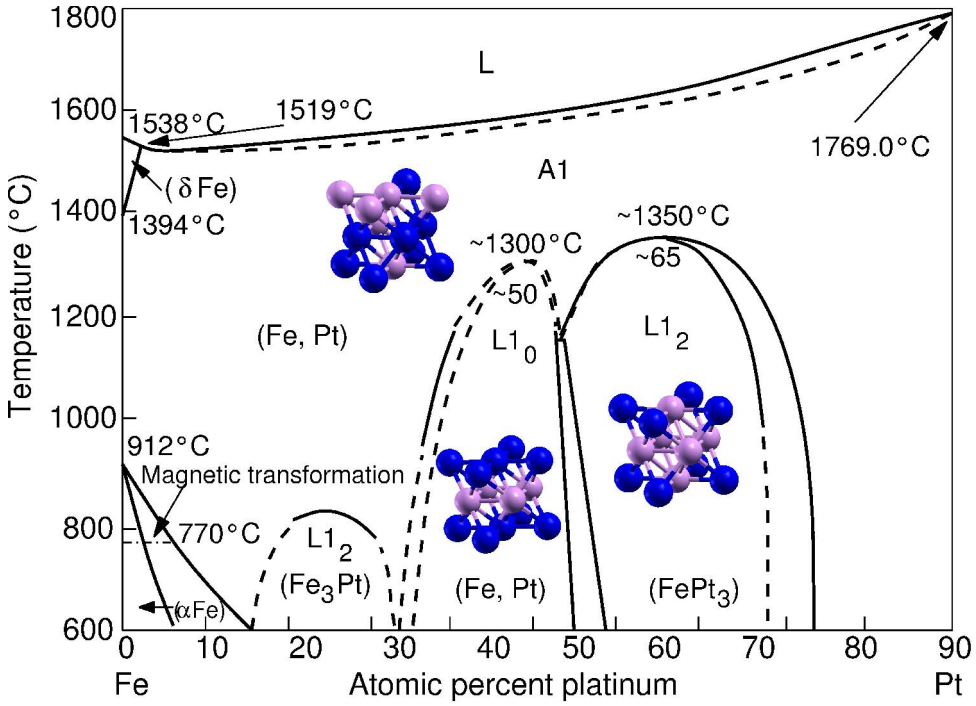

216x151mm (600 x 600 DPI)

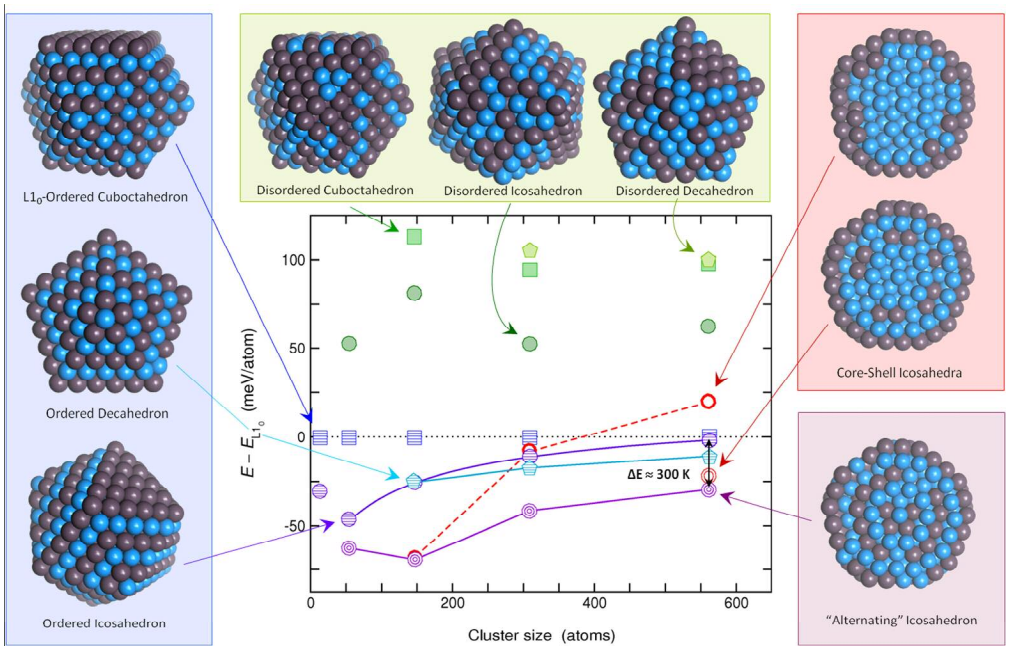

420x269mm (600 x 600 DPI)

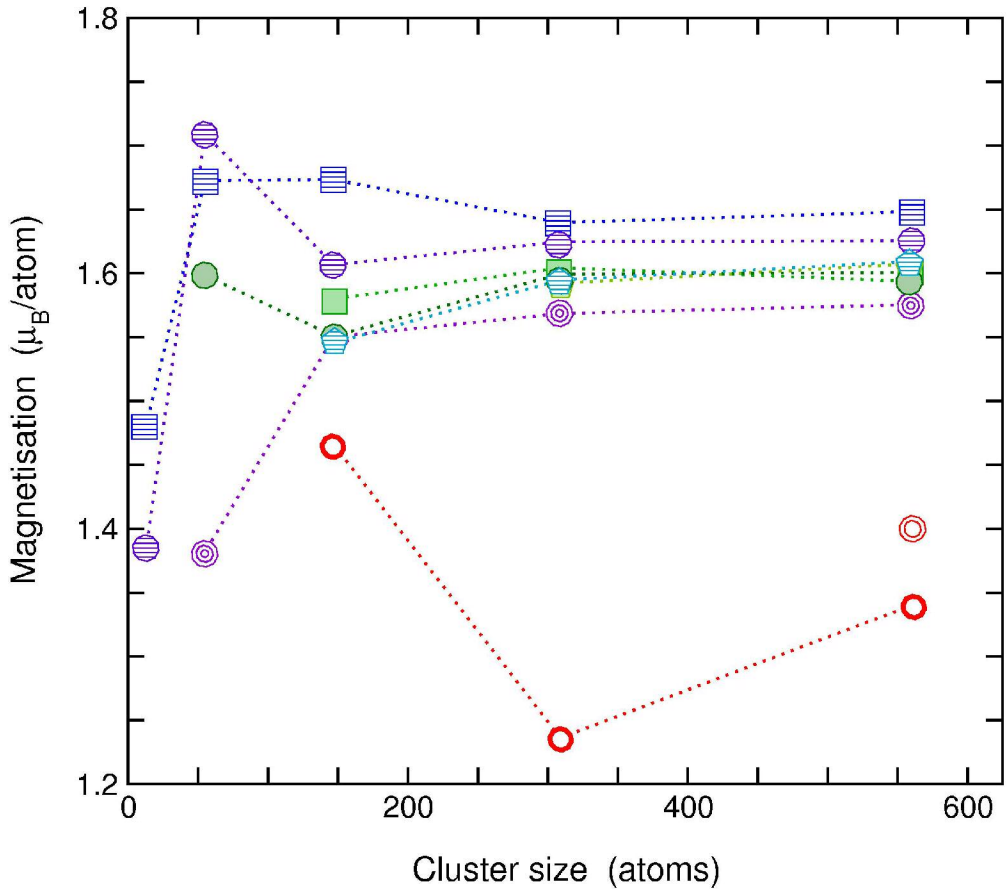

92x81mm (600 x 600 DPI)

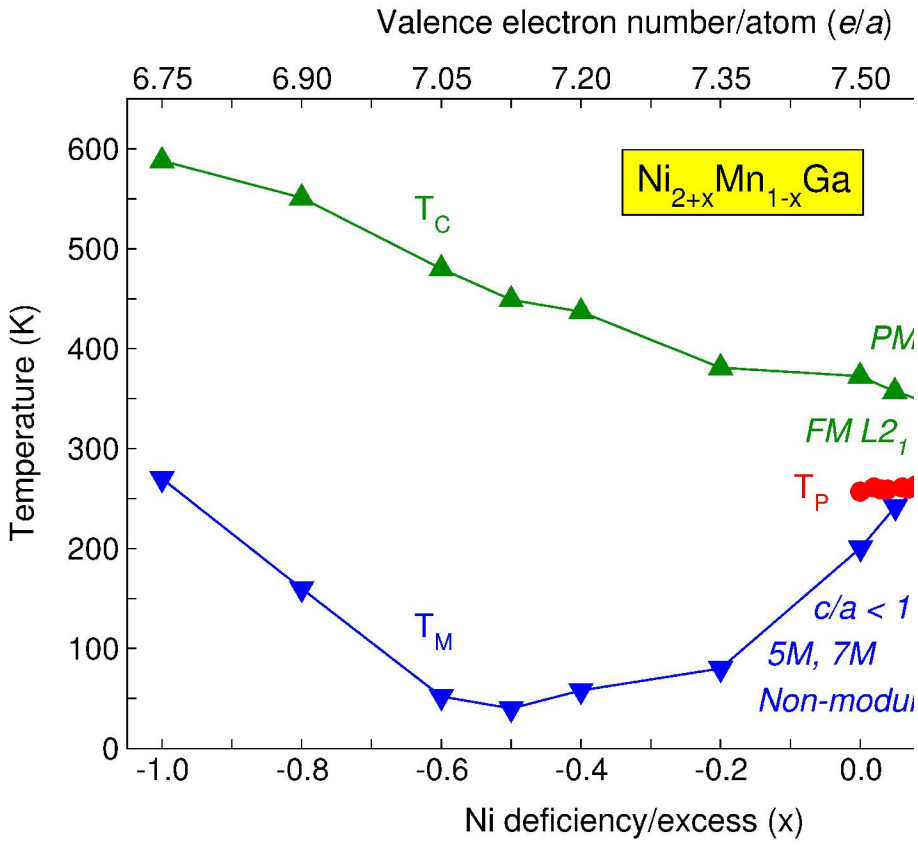

215x279mm (600 x 600 DPI)

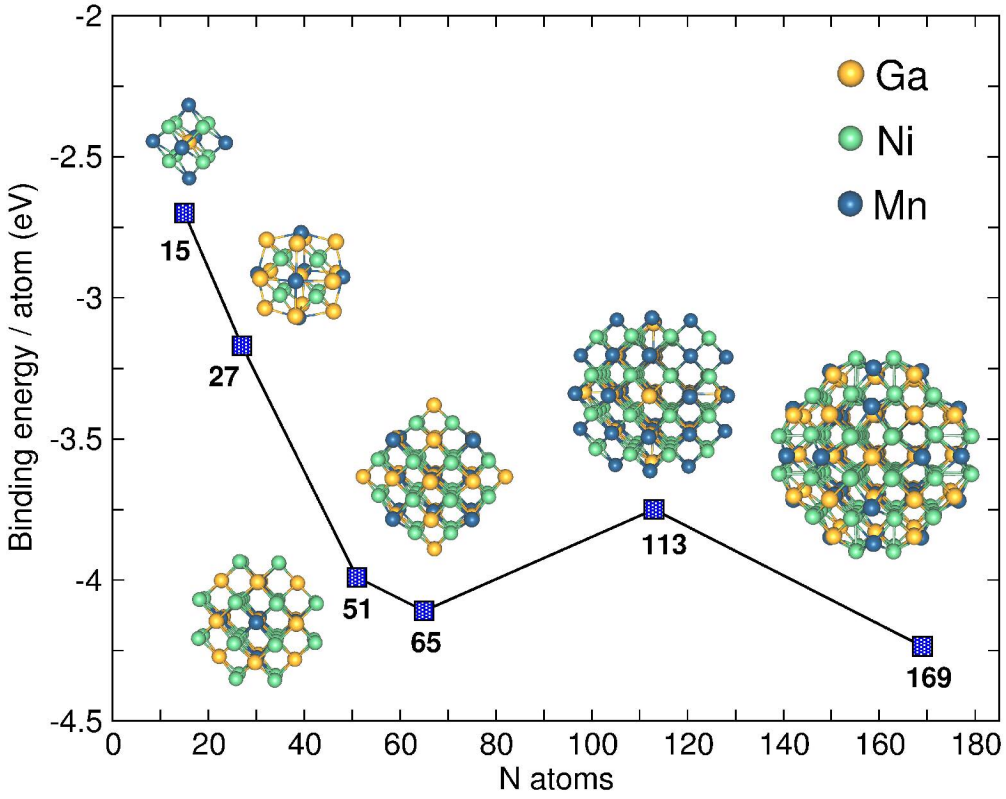

227x179mm (600 x 600 DPI)